

# Template Electrodeposition of Single-Phase p- and n-Type Copper Indium Diselenide (CuInSe<sub>2</sub>) Nanowire Arrays

Emil A. Hernández-Pagán, Wei Wang, and Thomas E. Mallouk\*

Department of Chemistry, The Pennsylvania State University, University Park, Pennsylvania 16802, United States

One-dimensional nano- and micro-structures are attractive architectures for solar energy applications, both because of the unique physical properties that emerge at the nanoscale and because of geometrical effects that influence the performance of photovoltaic and photoelectrochemical devices.<sup>1–5</sup> In the vertical wire array geometry the length scale of light absorption and charge separation can be independently controlled. That is, the thickness required to absorb the light can be matched by the length of the wires, while charge separation occurs in the orthogonal direction throughout the wire. In this geometry the minority carriers travel distances equal to or less than the wire radius, which should decrease charge recombination, especially in semiconductors with short minority carrier diffusion lengths. The fact that the minority carriers travel only a short distance can provide more flexibility in terms of the doping and the crystallinity (single crystal vs polycrystalline) of the materials used. Lewis and co-workers demonstrated that electrodeposited CdSe nanowire array photoelectrodes have a higher minority carrier collection efficiency and absorb lower energy photons more efficiently compared to planar photoelectrodes of similar thickness.<sup>4</sup> Also in a very elegant work, Fan and co-workers showed that a photovoltaic cell based on a n-CdS nanowires/p-CdTe junction had a higher efficiency ( $\eta \sim 6\%$ ) than a planar CdS/CdTe film of the same thickness, which they attributed to more efficient minority carrier collection.<sup>5</sup> In both of these experiments the nanowires were n-type. However it is more favorable in many applications to use p-type semiconductors in order to exploit the higher mobility and diffusion length of minority carrier electrons and to make photocathodes that are less susceptible to corrosion in liquid junctions.

**ABSTRACT** CuInSe<sub>2</sub> nanowire arrays were fabricated by electrodeposition from aqueous solutions of copper sulfate, indium sulfate, selenium dioxide, and citric acid, using anodic alumina membranes as templates. X-ray diffraction patterns showed that the wires were single phase (chalcopyrite structure) but polycrystalline, and a band gap of  $\sim 1$  eV was obtained from optical measurements. TEM and SEM confirmed that the grain size in nanowires annealed at 400 °C was in the range of 40 nm. The composition of the nanowires was uniform along the length of the wires and could be tuned by varying the electrodeposition potential. Analysis by ICP-MS showed that nanowires grown at  $-700$  mV were slightly Cu-rich, whereas those grown at  $-750$  mV were slightly In-rich. Mott–Schottky plots were employed to determine the doping type and flat band potential, verifying that the Cu- and In-rich wires were p- and n-type, respectively. Single-wire electrical transport measurements were also performed and showed that both types of wires had resistivities in the range  $10^{-1}–10^{-3} \Omega \cdot \text{cm}$ , consistent with carrier concentrations in the range  $10^{18}–10^{20} \text{ cm}^{-3}$ .

**KEYWORDS:** CuInSe<sub>2</sub> · nanowires · Mott–Schottky · electrodeposition

Although p-type nanowires can be fabricated by vacuum techniques (*i.e.*, VLS, CVD) and solution methods (*i.e.*, SLS, hydrothermal), the former is expensive in terms of capital equipment, and the latter presents challenges in terms of the dimensions and the assembly of the nanowires. In this regard, template-assisted electrodeposition is a versatile technique that has several advantages for making nanowire arrays. First it provides an easy way to control the dimensions of the nanowires, as the diameter is set by the pore size and the length can be controlled by the electrodeposition time. Second, the wires can be left in the template for array measurements, or they can be released for single wire measurements and characterization. Third, it is an inexpensive technique and provides a high density of wires ( $\sim 10^9$ ). However, most of the semiconductor nanowires reported in the literature that can be easily electrodeposited and have band gaps that match the solar spectrum are n-type.

Copper indium diselenide (CuInSe<sub>2</sub>) has been extensively studied and widely used in solar cells. It has a direct band gap of 1 eV,

\* Address correspondence to tem5@psu.edu.

Received for review January 29, 2011 and accepted March 3, 2011.

Published online March 03, 2011  
10.1021/nn200373k

© 2011 American Chemical Society

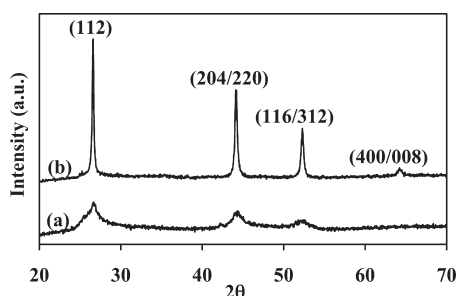


Figure 1. XRD pattern of  $\text{CuInSe}_2$  nanowires: (a) as-deposited, (b) annealed at  $400^\circ\text{C}$ .

which matches the solar spectrum well, and it can be made by electrodeposition with n- or p-type doping. Photovoltaic cells based on polycrystalline films of  $\text{CuInSe}_2$  have been reported with efficiencies as high as 15%.<sup>6</sup> Several groups have reported the synthesis of nanostructures using solution routes and their use in solar devices.<sup>7–12</sup> Phok *et al.* first reported the electrodeposition of  $\text{CuInSe}_2$  nanowires by a pulse electrodeposition method.<sup>13</sup> However they did not present full characterization of the wires, and no devices based on these nanowires were reported. Here we report the fabrication of p- and n-type  $\text{CuInSe}_2$  nanowire arrays by a one-step electrodeposition route, as well as their full characterization.

## RESULTS AND DISCUSSION

Figure 1 shows the XRD patterns of as-deposited and annealed  $\text{CuInSe}_2$  nanowires embedded in the amorphous alumina membrane after dissolving the gold layer. The pattern corresponds to the chalcopyrite structure and can be indexed to the (112), (204/220), (116/312), and (400/008) crystal planes. For the as-deposited nanowires an average crystallite size was calculated from the Scherrer equation, eq 1, where  $\lambda$  is the X-ray wavelength in angstroms ( $1.54056 \text{ \AA}$ ),  $\beta$  is the width of the XRD peak at half its height in radians, and  $\theta_\beta$  is the position of the peak (note:  $\theta$ , not  $2\theta$ ). For the as-deposited nanowires, based on the first peak at  $26.59 2\theta$ , a  $\theta$  of  $13.295^\circ$  and a  $\beta$  of  $0.074$  were obtained, giving a  $2 \text{ nm}$  crystalline domain size. After annealing, using the same peak, a crystallite size of  $\sim 40 \text{ nm}$  ( $\beta = 0.0037$ ) was calculated.

Individual wires were studied by etching the alumina membranes in aqueous  $\text{NaOH}$ , followed by several centrifugation cycles in deionized water. Our previous experience with the template synthesis of nanowires shows that the forces involved in centrifugation can cause soft metal or polymer wires to bend and that polycrystalline semiconductor wires can break into fragments.<sup>14</sup> After annealing, mostly intact  $\text{CuInSe}_2$  wires were found in this study, indicating good mechanical integrity. Examination of the annealed nanowires with dark field TEM (Figure 2a,b) reveals crystallites of the size calculated from the XRD pattern.

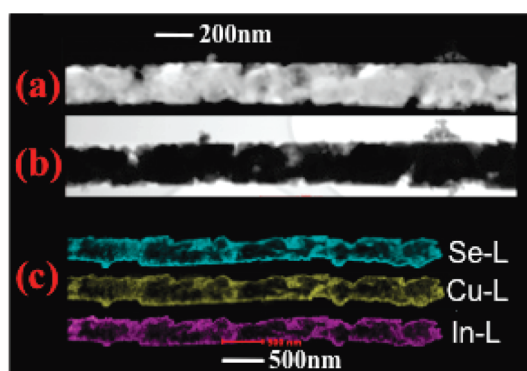


Figure 2. Transmission electron micrographs of  $\text{CuInSe}_2$  nanowires showing larger grains after annealing: (a) dark field image, (b) bright field image. (c) TEM/EDS map showing uniform elemental distribution.

The deleterious effects that small grains have on the performance of photovoltaic and photoelectrochemical cells are well documented in the literature. In a recent paper by Schierhorn and co-workers on  $\text{CdSe}$  nanorod array photoelectrodes they estimated that their as-electrodeposited rods had a grain density 1300 times that of annealed rods at  $500^\circ\text{C}$ .<sup>3</sup> Given that the crystallite sizes of their as-deposited and annealed rods are close to those reported here, a similar grain density is expected. Therefore electrical measurements were performed on the annealed nanowires.

$$L = \frac{0.94\lambda}{\beta \cos \theta_\beta} \quad (1)$$

Another important factor that can affect the performance of compound semiconductors is their stoichiometry and, in ternary and quaternary semiconductors in particular, phase separation. When electrodepositing  $\text{CuInSe}_2$ , it has been reported that the mechanism involves the formation of the binary phases  $\text{Cu}_x\text{Se}$  and  $\text{In}_y\text{Se}$ , which combine to form the ternary semiconductor.<sup>13,15,16</sup> Nonstoichiometric deposits can result in the ternary phase with a binary phase as an impurity. The effects that these phase impurities have on the properties and performance of solar cells based on  $\text{CuInSe}_2$  are reduction of the photoactive volume, increase in the boundary charge recombination, lower absorption coefficient, among others (for details see refs 17–19). From the XRD pattern it can be seen that within the detection limits there are no other phases present in our samples. This is further supported by TEM/EDS mapping, which shows a uniform elemental distribution throughout the wires (Figure 2c). Also the optical spectrum shows a transition around  $1200 \text{ nm}$  corresponding to a  $1.0 \text{ eV}$  band gap, which is in agreement with the value reported in the literature.<sup>18,20</sup>

To determine the stoichiometry of the nanowires, they were dissolved and the resulting solution was analyzed with ICP-MS (Table 1). Nanowires

electrodeposited at  $V_{\text{sce}} = -600$  mV were Cu-rich, whereas  $V_{\text{sce}} = -700$  mV gave stoichiometric wires that were slightly Cu-rich. Changing the electrodeposition potential by  $-50$  mV also results in stoichiometric wires, but in this case slightly In-rich. These results are consistent with the electrodeposition of Cu, Se, and In at  $V_{\text{sce}} = -600$  mV,  $V_{\text{sce}} = -700$  mV, and  $V_{\text{sce}} = -800$  mV for  $\text{Cu}^{2+}$ -citrate complex,  $\text{H}_2\text{SeO}_3$ , and  $\text{In}^{3+}$ -citrate complex, respectively.<sup>21–23</sup>

It has been established that slightly Cu-rich  $\text{CuInSe}_2$  is p-type, whereas slightly In-rich  $\text{CuInSe}_2$  is n-type.<sup>24,25</sup> To confirm that the samples deposited at  $V_{\text{sce}} = -700$  mV and  $V_{\text{sce}} = -750$  mV were p-type and n-type, respectively, Mott–Schottky (M–S) analysis was employed. The Mott–Schottky analysis is based on the relationship between the space charge layer capacitance and the applied potential, as given by eq 2. Here  $C$  is the capacitance of the space charge layer,  $e$  the elementary charge,  $\epsilon$  the dielectric constant of the semiconductor,  $\epsilon_0$  the permittivity,  $A$  the surface area,  $N$  the carrier concentration,  $V$  the applied potential,  $V_{\text{FB}}$  the flat band potential,  $k$  the Boltzmann constant, and  $T$  the temperature.<sup>26,27</sup>

$$\frac{1}{C^2} = \left( \frac{2}{e\epsilon\epsilon_0NA^2} \right) \left( V - V_{\text{FB}} - \frac{kT}{e} \right) \quad (2)$$

The M–S analysis allows one to determine  $V_{\text{FB}}$  by extrapolating to the intercept of the potential axis, and the carrier concentration can be calculated if the surface area is known. Also the slope (negative or positive) provides information on the carrier type. Figure 4a shows the M–S plot for a sample deposited at

**TABLE 1. Composition Determined by ICP-MS for Wires Deposited at Different Potentials**

deposition potential (vs SCE)	Cu (mol)	In (mol)	Se (mol)	stoichiometry
$-600$ mV	$6.77 \times 10^{-7}$	$4.44 \times 10^{-7}$	$4.18 \times 10^{-7}$	1.60:1.06:1.00
$-700$ mV	$8.65 \times 10^{-7}$	$8.27 \times 10^{-7}$	$1.67 \times 10^{-6}$	1.04:1.00:2.02
$-750$ mV	$6.77 \times 10^{-7}$	$7.31 \times 10^{-7}$	$1.45 \times 10^{-6}$	1.00:1.08:2.14

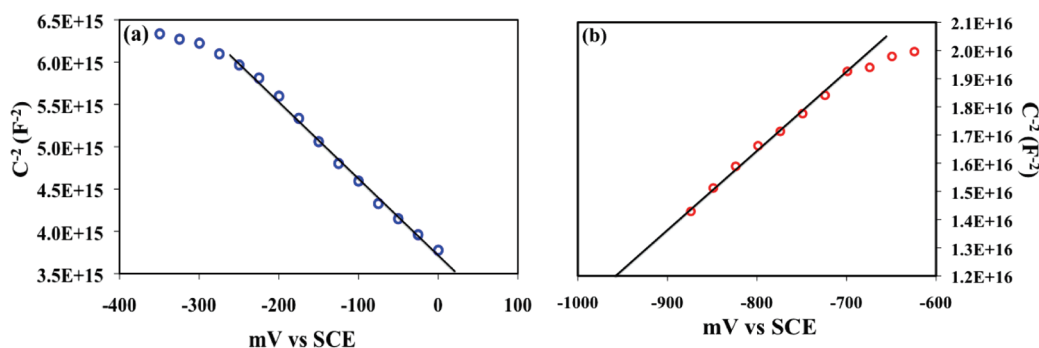
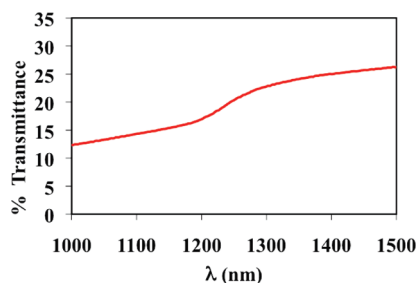


**Figure 4.** Mott–Schottky plots for  $\text{CuInSe}_2$  nanowires film on Mo foil in 100 mM  $\text{LiClO}_4$  in acetonitrile, 10 mV ac signal, and 1 kHz. Nanowires deposited at (a)  $V_{\text{sce}} = -700$  mV and (b)  $V_{\text{sce}} = -750$  mV.

$V_{\text{sce}} = -700$  mV. It can be seen that the plot has a negative slope, as expected for a p-type material, and  $V_{\text{FB}} \approx 15$  mV, corresponding to the position of the valence band. For samples deposited at  $V_{\text{sce}} = -750$  mV (Figure 4b) a positive slope is obtained, with a  $V_{\text{FB}} \approx -950$  mV, corresponding to the position of the conduction band. Both  $V_{\text{FB}}$  values are in agreement with values reported in the literature.<sup>28–30</sup> Since the surface area is not known for our samples, we could not determine the carrier concentration by this method. However an estimate carrier concentration was obtained with electrical measurements.

It is important to mention that the electrical transport measurements were performed only on p-type wires because our future goal is to fabricate photovoltaic cells with a Mo/p- $\text{CuInSe}_2$ NWs/CdS/ZnO configuration, which is the most common one for this material. First, the  $i$ – $V$  properties of individual wires were measured while applying a gate voltage. The  $i$ – $V$  properties were independent of the gate voltage applied, suggesting that the nanowires are heavily doped (Figure S4). Four-point probe measurements were also employed, and the results are presented in Table 2. The resistance,  $R$ , was determined from the slope of the  $i$ – $V$  curve, and the resistivity,  $\rho$ , was calculated with dimensions obtained from SEM images. A hole mobility,  $\mu_{\text{hr}}$ , of  $10 \text{ cm}^2 \text{ V}^{-1} \text{ s}^{-1}$  was used to estimate the carrier concentrations.<sup>25</sup>

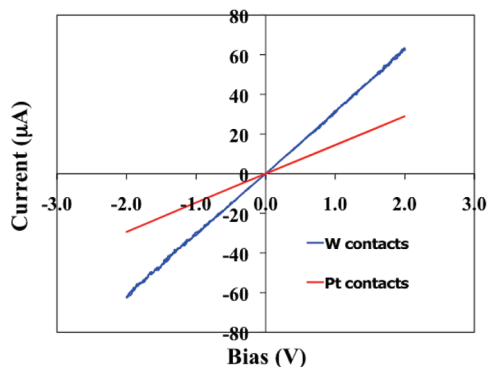
From these measurements it was determined that most of the wires fall within a range of resistivity on the



**Figure 3.** Optical spectrum of drop-cast nanowires showing a transition close to 1200 nm, corresponding to a 1 eV band gap.

**TABLE 2. Results from Single-Wire Electrical Measurements**

sample	$R$ (ohm)	$\rho$ (ohm·cm)	carrier
			concentration ( $\text{cm}^{-3}$ )
nanowire 1	$2.9 \times 10^4$	$2.1 \times 10^{-1}$	$3.0 \times 10^{18}$
nanowire 2	$2.02 \times 10^2$	$1.1 \times 10^{-3}$	$5.5 \times 10^{20}$
nanowires 3–8	$(1–9.7) \times 10^3$	$(1–7.5) \times 10^{-2}$	$(2–8.4) \times 10^{19}$

**Figure 5. Single-wire four-point measurements with different contacts, showing ohmic behavior.**

order of  $10^{-2}$  ohm·cm. The differences in the values obtained can be a result of different roughness, different level of defects, carrier mobility variations between wires, among other factors. However the estimated carrier concentrations indicate that the wires are heavily doped, which is consistent with the results obtained by gate-dependent measurements. Further, these values fall within those reported by several authors for electrodeposited films.<sup>24,31</sup> In addition, Figure 5 illustrates

that there is ohmic contact between the wires and the high work function metal electrodes (Pt, W), which is as expected for p-type wires. As a proof of concept, devices with the configuration Mo/p-CuInSe<sub>2</sub>NWs/CdS/ZnO/ITO were made by drop-casting the nanowires onto Mo foil (see Supporting Information). The  $i$ - $V$  power curves obtained from these devices show a photoresponse dominated by resistance (Figure S6). We attribute this to several factors. First, the sputtered top contacts were not continuous (Figure S5). Second, the sputtering conditions for the top contacts were not optimized, and thus the sputtered films were highly resistive. Finally, drop-casting results in a tortuous path for charge transport compared to vertically aligned nanowires. Future work will focus on improving these parameters for nanowire array solar cells.

## CONCLUSIONS

CuInSe<sub>2</sub> nanowires were fabricated through a one-step electrodeposition process. The resulting wires are single-phase chalcopyrite and have a composition near the ideal 1:1:2 stoichiometry. The as-deposited nanowires have poor crystallinity, which readily improves upon annealing. The wires can be grown p- or n-type by adjusting the electrodeposition potential, which was confirmed by Mott–Schottky analysis. This analysis also allowed the determination of the flat band potential for both types of samples. Electrical measurements performed on individual wires revealed that the wires are heavily doped and have ohmic behavior when contacted with high work function metals, as expected for p-type samples. Future work will focus on making solar devices based on vertical nanowire arrays.

## MATERIALS AND METHODS

**Fabrication.** Whatman Anodisc alumina membranes with a nominal pore diameter of 200 nm were used as templates. Previous experiments with metal and polymer electrodeposition in these membranes have shown that the pore diameter is actually *ca.* 350 nm, but that the pores are branched and narrower on one side of the membrane.<sup>14</sup> A gold layer of 150 nm was thermally evaporated on one side of the membrane and served as the working electrode. Prior to the electrodeposition of CuInSe<sub>2</sub> a sacrificial layer of Au was electrodeposited at a constant current density of 0.67 mA/cm<sup>2</sup> for 1 h to fill the branched region of the membrane. A coiled platinum wire and a saturated calomel electrode (SCE) served as the counter and reference electrodes, respectively, when depositing the nanowires. The electrolyte used consisted of 3 mM CuSO<sub>4</sub>·5H<sub>2</sub>O, 3 mM In<sub>2</sub>(SO<sub>4</sub>)<sub>3</sub>·nH<sub>2</sub>O, 5 mM SeO<sub>2</sub>, and 0.1 M citric acid. The potential used was either -700 or -750 mV vs SCE. Once the CuInSe<sub>2</sub> nanowires were electrodeposited, the sacrificial Au backing and electrodeposited Au layer were removed using a commercial Au etchant (Transene GE-8148, 5 min). Afterward the samples were rinsed with copious amounts of water followed by ethanol. The samples were then annealed in a tube furnace at 400 °C for 15 min under nitrogen flow.

**Characterization.** X-ray diffraction patterns were obtained using Cu K $\alpha_1$  radiation on a Philips X'pert MPD system while the wires were embedded in the template. The wires were released from the template for SEM/EDS (FEI Quanta 200 ESEM), TEM/EDS (JEOL 2010F), and optical characterization (Perkin-Elmer Lambda 950) by dissolving the alumina in 5 M NaOH and were cleaned with several cycles of centrifugation in H<sub>2</sub>O until the supernatant had a neutral pH. For ICP-MS analysis (X-Series 2 ICPMS with Collision Cell Technology, Thermo, Fisher Scientific) the wires were dissolved in 143  $\mu$ L of concentrated HNO<sub>3</sub> and diluted to a final volume of 5 mL with H<sub>2</sub>O to make a 2% HNO<sub>3</sub> matrix. Mott–Shottky analysis was performed by drop-casting the nanowires onto a molybdenum foil that was insulated with epoxy. The electrolyte used was 100 mM LiClO<sub>4</sub> in acetonitrile, the amplitude of the ac signal was 10 mV, and the frequency was 1 kHz. Platinum or tungsten electrical contacts to individual wires were made with a focused ion beam (FEI Quanta 200 3D). Nanowires were cast onto a n++ Si wafer coated with a 120 nm silicon nitride layer that served as the dielectric and a Ti(30 nm)/Au(100 nm) layer on the other side that served as the back gate. For the electrical measurements, a Cascade Microtech Summit 12000 probe station was used coupled to two high-impedance Keithley 6514 System electrometers connected to the voltage measurement units of an Agilent 4516B semiconductor parameter analyzer.

**Acknowledgment.** This work was supported by the Office of Basic Energy Sciences, Division of Chemical Sciences, Geosciences, and Energy Biosciences, Department of Energy, under contract DE-FG02-07ER15911. SEM, TEM, and FIB were performed at the Materials Characterization Facility at the Penn State Materials Research Institute. The authors thank Aaron Vallett and Meng-Wei Kuo for their help in the four-point probe measurements, and Dr. Greg Barber for his assistance during the solar measurements.

**Supporting Information Available:** Scanning electron microscope images and EDS spectra of  $\text{CuInSe}_2$  nanowires, SEM images of individual wires aligned for four-point conductivity measurements, conductivity data, fabrication details of thin film photovoltaic devices, and electrical characterization. This material is available free of charge via the Internet at <http://pubs.acs.org>.

## REFERENCES AND NOTES

- Kayes, B. M.; Atwater, H. A.; Lewis, N. S. Comparison of the Device Physics Principle of Planar and Radial p-n Junction Nanorod Solar Cells. *J. Appl. Phys.* **2005**, *97*, 114302–1–11.
- Goodey, A. P.; Eichfeld, S. M.; Lew, K.; Redwing, J. M.; Mallouk, T. E. Silicon Nanowire Array Photoelectrochemical Cells. *J. Am. Chem. Soc.* **2007**, *129*, 12344–12345.
- Schierhorn, M.; Boettcher, S. W.; Kraemer, S.; Stucky, G. D.; Moskovits, M. Photoelectrochemical Performance of  $\text{CdSe}$  Nanorod Arrays Grown on a Transparent Conducting Substrate. *Nano Lett.* **2009**, *9*, 3262–3267.
- Spurgeon, J. M.; Atwater, H. A.; Lewis, N. S. A Comparison between the Behavior of Nanorod Array and Planar  $\text{Cd}(\text{Se}, \text{Te})$  Photoelectrodes. *J. Phys. Chem. C* **2008**, *112*, 6186–6193.
- Fan, Z.; Razavi, H.; Do, J.; Moriwaki, A.; Ergen, O.; Chueh, Y.; Leu, P. W.; Ho, J. C.; Takahashi, T.; Reichertz, L. A.; et al. Three-Dimensional Nanopillar-Array Photovoltaics on Low-Cost and Flexible Substrates. *Nat. Mater.* **2009**, *8*, 648–653.
- AbuShama, J. A. M.; Johnston, S.; Moriarty, T.; Teeter, G.; Ramanathan, K.; Noufi, R. Properties of  $\text{ZnO}/\text{CdS}/\text{CuInSe}_2$  Solar Cells with Improved Performance. *Prog. Photovoltaics: Res. Appl.* **2004**, *12*, 39–45.
- Xu, J.; Luan, C.-Y.; Tang, Y.-B.; Chen, X.; Zapfen, J. A.; Zhang, W.-J.; Kwong, H.-L.; Meng, X.-M.; Lee, S.-T.; Lee, C.-S. Low Temperature Synthesis of  $\text{CuInSe}_2$  Nanotube Array on Conducting Glass Substrates for Solar Cell Applications. *ACS Nano* **2010**, *2*, 6064.
- Wang, J.-J.; Wang, Y.-Q.; Cao, F.-F.; Guo, Y.-G.; Wan, J. J. Synthesis of Monodispersed Wurtzite Structure  $\text{CuInSe}_2$  Nanocrystals and Their Application in High-Performance Organic–Inorganic Hybrid Photodetectors. *J. Am. Chem. Soc.* **2010**, *132*, 12218–12221.
- Panthani, M. G.; Akhavan, V. A.; Goodfellow, B. W.; Schmidtke, J. P.; Dunn, L.; Dodabalapur, A.; Barbara, P. F.; Korgel, B. A. Synthesis of  $\text{CuInS}_2$ ,  $\text{CuInSe}_2$ , and  $\text{Cu}(\text{In}_x\text{Ga}_{1-x})\text{Se}_2$  (CIGS) Nanocrystal “Inks” for Printable Photovoltaics. *J. Am. Chem. Soc.* **2008**, *130*, 16770–16777.
- Yang, Y.; Chen, Y. Solvothermal Preparation and Spectroscopic Characterization of Copper Indium Diselenide Nanorods. *J. Phys. Chem. B* **2006**, *110*, 17370–17374.
- Guo, Q.; Kim, S. J.; Kar, M.; Shafarman, W. N.; Birkmire, R. W.; Stach, E. A.; Agrawal, R.; Hillhouse, H. W. Development of  $\text{CuInSe}_2$  Nanocrystal and Nanoring Inks for Low-Cost Solar Cells. *Nano Lett.* **2008**, *8*, 2982–2987.
- Koo, B.; Patel, R. N.; Korgel, B. A. Synthesis of  $\text{CuInSe}_2$  Nanocrystals with Trigonal Pyramidal Shape. *J. Am. Chem. Soc.* **2009**, *131*, 3134–3135.
- Phok, S.; Rajaputra, S.; Singh, V. P. Copper Indium Diselenide Nanowire Arrays by Electrodeposition in Porous Alumina Templates. *Nanotechnology* **2007**, *18*, 475601.
- Kline, T. R.; Tian, M.; Wang, J.; Sen, A.; Chan, M. W. H.; Mallouk, T. E. Template Grown Metal Nanowires. *Inorg. Chem.* **2006**, *45*, 7555–7565.
- Guillemoles, J.; Cowache, P. C.; Lusson, A.; Fezzaa, K.; Boisvion, F.; Vedel, J.; Lincot, D. One Step Electrodeposition of  $\text{CuInSe}_2$ : Improved Structural, Electronic, and Photovoltaic Properties by Annealing under High Selenium Pressure. *J. Appl. Phys.* **1996**, *79*, 7293–7302.
- Pern, F. J.; Noufi, R.; Mason, A.; Franz, A. Characterizations of Electrodeposited  $\text{CuInSe}_2$  Thin Films: Structure, Deposition and Formation Mechanisms. *Thin Solid Films* **1991**, *202*, 299–314.
- Tuttle, J. R.; Albin, D. S.; Noufi, R. Thoughts on the Microstructure of Polycrystalline Thin Film  $\text{CuInSe}_2$  and Its Impact on Material and Device Performance. *Sol. Cells* **1991**, *30*, 21–38.
- Guillen, C.; Herrero, J. Optical Properties of Electrochemically Deposited  $\text{CuInSe}_2$  Thin Films. *Sol. Energy Mater. Sol. Cells* **1991**, *23*, 31–45.
- Schmid, D.; Ruckh, M.; Grunwald, F.; Schock, H. W. Chalcopyrite/Defect Chalcopyrite Heterojunctions on the Basis of  $\text{CuInSe}_2$ . *J. Appl. Phys.* **1993**, *73*, 2902–2908.
- Gujar, T. P.; Shinde, V. R.; Park, J.; Lee, H. K.; Jung, K.; Joo, O. Characterization of Electrochemically Grown Crystalline  $\text{CuInSe}_2$  Thin Films. *J. Electrochem. Soc.* **2009**, *156*, E8–E12.
- Kazacos-Skyllas, M.; Miller, B. Studies in Selenious Acid Reduction and  $\text{CdSe}$  Film Deposition. *J. Electrochem. Soc.* **1980**, *127*, 869–873.
- Herrero, J.; Ortega, J. Electrodeposition of Cu–In Alloys for Preparing  $\text{CuInS}_2$  Thin Films. *Sol. Energy Mater.* **1990**, *20*, 53–65.
- Guillen, C.; Galiano, E.; Herrero, J. Cathodic Electrodeposition of  $\text{CuInSe}_2$  Thin Films. *Thin Solid Films* **1991**, *195*, 137–146.
- Rockett, A.; Birkmire, R. W.  $\text{CuInSe}_2$  for Photovoltaic Applications. *J. Appl. Phys.* **1991**, *70*, R81–R97.
- Wagner, S.; Bridenbaugh, P. M. Multicomponent Tetrahedral Compounds for Solar Cells. *J. Cryst. Growth* **1977**, *39*, 151–159.
- Bard, A. J.; Faulkner, L. F., *Electrochemical Methods: Fundamentals and Applications*, second ed.; John Wiley & Sons: New York, 2001.
- Sebastian, P. J.; Calixto, M. E.; Bhattacharya, R. N.; Noufi, R. CIS and CIGS Based Photovoltaic Structures Developed from Electrodeposited Precursors. *Sol. Energy Mater. Sol. Cells* **1999**, *59*, 125–135.
- Lincot, D.; Gomez-Meier, H.; Kessler, J.; Vedel, J. Photoelectrochemical Study of p-Type Copper Indium Diselenide Thin Films for Photovoltaic Applications. *Sol. Energy Mater.* **1990**, *20*, 67–79.
- Singh, R. P.; Singh, S. L. Electrodeposited Semiconducting  $\text{CuInSe}_2$  Films: II. Photo-electrochemical Solar Cells. *J. Phys. D: Appl. Phys.* **1986**, *19*, 1759–1769.
- Ye, H.; Park, H. S.; Akhavan, V. A.; Goodfellow, B. W.; Panthani, M. G.; Korgel, B. A.; Bard, A. J. Photoelectrochemical Characterization of  $\text{CuInSe}_2$  and  $\text{Cu}(\text{In}_{1-x}\text{Ga}_x)\text{Se}_2$  Thin Films For Solar Cells. *J. Phys. Chem. C* **2011**, *115*, 234–240.
- Varela, M.; Morenza, J. L.; Esteve, J.; Codina, J. M. Electrical Conductivity of Polycrystalline  $\text{CuInSe}_2$  Thin Films. *J. Phys. D: Appl. Phys.* **1984**, *17*, 2423–2427.